



## What does airborne LiDAR really measure in upland ecosystems?

Journal:	<i>Ecohydrology</i>
Manuscript ID:	ECO-13-0201.R1
Wiley - Manuscript type:	Research Article
Date Submitted by the Author:	20-Jun-2014
Complete List of Authors:	Luscombe, David; University of Exeter, Geography, College of Life and Environmental Sciences Anderson, Karen; University of Exeter, Environment and Sustainability Institute Gatis, Naomi; University of Exeter, Geography, College of Life and Environmental Sciences Wetherelt, Andy; University of Exeter, Camborne School of Mines Grand-Clement, Emilie; University of Exeter, Geography, College of Life and Environmental Sciences Brazier, Richard; University of Exeter, Geography, College of Life and Environmental Sciences
Keywords:	LiDAR, Peatlands, Terrestrial Laser Scanning, Ecosystem services

SCHOLARONE™  
Manuscripts

ew

1  
2  
3  
4  
5  
6  
7  
8  
9  
10  
11  
12  
13  
14  
15  
16  
17  
18  
19  
20  
21  
22  
23  
24  
25  
26  
27  
28  
29  
30  
31  
32  
33  
34  
35  
36  
37  
38  
39  
40  
41  
42  
43  
44  
45  
46  
47  
48  
49  
50  
51  
52  
53  
54  
55  
56  
57  
58  
59  
60

# What does airborne LiDAR really measure in upland ecosystems?

June 2014

David J Luscombe<sup>1</sup>, Karen Anderson<sup>2</sup>, Naomi Gatis<sup>1</sup>, Andy Wetherelt<sup>3</sup>, Emilie Grand-Clement<sup>1</sup> and Richard E Brazier<sup>1</sup>

*Corresponding author: David J Luscombe, Email:d.j.luscombe@exeter.ac.uk,  
Tel:07748968462*

<sup>1</sup> Geography, CLES, University of Exeter, Amory Building, Rennes Drive, Exeter, Devon EX4 4RG

<sup>2</sup> Environment and Sustainability Institute, University of Exeter, Cornwall Campus, Treliiever Road, Penryn, Cornwall, TR10 9EZ

<sup>3</sup> Camborne School of Mines, University of Exeter (Cornwall Campus), Tremough Penryn, Cornwall, TR10 9EZ

1  
2  
3  
4 **1 ABSTRACT**

5  
6 Airborne laser scanning systems (LiDAR) are very well suited to the study of landscape and  
7  
8 vegetation structure over large extents. Spatially distributed measurements describing the 3D  
9  
10 character of landscape surfaces and vegetation architecture can be used to understand eco-  
11  
12 geomorphic and ecohydrological processes, and this is particularly pertinent in peatlands given  
13  
14 the increasing recognition that these landscapes provide a variety of ecosystem services (water  
15  
16 provision, flood mitigation, carbon sequestration). In using LiDAR data for monitoring  
17  
18 peatlands, it is important to understand how well peatland surface structures (with fine length  
19  
20 scales) can be described. Our approach integrates two laser scanning technologies, namely  
21  
22 Terrestrial Laser Scanning and airborne LiDAR surveys, to assess how effective airborne  
23  
24 LiDAR is at measuring these fine scale microtopographic ecohydrological structures. By  
25  
26 combining airborne and terrestrial laser scanning, we demonstrate an improved spatial  
27  
28 understanding of the signal measured by the airborne LiDAR. Critically, results demonstrate  
29  
30 that LiDAR DSMs are subject to specific errors related to short-sward ecosystem structure,  
31  
32 causing the vegetation canopy height and surface-drainage network depth to be underestimated.  
33  
34 TLS is shown to be effective at describing these structures over small extents, allowing the  
35  
36 information content and accuracy of airborne LiDAR to be understood and quantified more  
37  
38 appropriately. These findings have important implications for the appropriate degree of  
39  
40 confidence ecohydrologists can apply to such data when using them as a surrogate for field  
41  
42 measurements. They also illustrate the need to couple LiDAR data with ground validation data  
43  
44 in order to improve assessment of ecohydrological function in such landscapes.  
45  
46  
47  
48  
49  
50

51 **Keywords: LiDAR, Terrestrial Laser Scanning, DSM, Uncertainty, Peatlands, Uplands,**  
52 **Ecohydrology, Ecosystem services, Exmoor, UK.**  
53  
54  
55  
56  
57  
58  
59  
60

## 23 INTRODUCTION

24 There is a new monitoring imperative for peatlands as global policy recognises the importance  
25 of these ecosystems in tackling climate change, water management objectives and biodiversity  
26 conservation (Bain et al. 2011; Grand-Clement et al. 2013). Spatially distributed measurements  
27 from airborne laser scanning systems such as Airborne Light Detection And Ranging (LiDAR),  
28 are useful for describing the three dimensional structure of landscape surfaces and vegetation  
29 (Emanuel 2013; Hutton and Brazier 2012; Mitchell et al. 2012; Rango et al. 2000; Zimble et al.  
30 2003), and there is considerable evidence that such data provide valuable information on  
31 ecohydrological and eco-geomorphic processes in peatlands (Korpela et al. 2009; Anderson &  
32 Bennie 2010). In addition, landscape and ecosystem structure have long been recognised as  
33 important controls on peatland function (Moore and Bellamy 1974; Barber 1981). More  
34 recently Belyea and Clymo (2001) have explored the link between microtopography and peat  
35 formation and the *ecohydrology* of mires, leading to the contemporary understanding of links  
36 between microtopography and ecohydrological functioning summarised by Holden (2005) and  
37 Lindsay (2010).

38 The use of laser scanning techniques in peatlands could permit the quantification of how  
39 peatland structure and function change through time, leading to a dynamic understanding of  
40 landscape-scale ecohydrological behaviour (Fisher et al. 2009; Lane and D'Amico 2010;  
41 Turnbull et al. 2008). However, progress towards this in an operational sense is limited by our  
42 understanding of what the LiDAR signal actually represents in real terms – e.g. can LiDAR  
43 deliver robust measurements of both the short-sward canopy and/or the landscape surface?  
44 Spatially distributed information on both of these factors is needed because many temperate  
45 peatlands are dominated by low sward vegetation (Drewitt and Manley 1997) with structurally  
46 subtle micro-topographic features (Kincey and Challis 2009; Lindsay 2010): both of which  
47 impart significant effects on the ecohydrological functioning of peatlands (Holden et al. 2004).

1  
2  
3 48 Small shifts in ecological structure or drainage pattern may, for example, elicit major shifts in  
4  
5 49 the hydrological response of the system.  
6  
7

8 50 LiDAR technologies use a precisely timed laser pulse and measure the return signal to capture  
9  
10 51 accurate altimetry measurements of the Earth's surface, over large spatial extents. When  
11  
12 52 analysing LiDAR datasets at landscape scales, there is often an assumption that the data are  
13  
14 53 directly representative of the 3-D habitat structure (e.g. forest canopy) or the true ground  
15  
16 54 surface (Jones et al. 2008; Kincey and Challis 2009). For example, LiDAR-derived digital  
17  
18 55 surface models (DSMs) are often used to calculate hillshade products (Barbier et al. 2011;  
19  
20 56 Kincey and Challis 2009), canopy height models for forestry (Zimble et al. 2003), or used to  
21  
22 57 support numerical models of wetness, surface roughness or surface flows. (Beven 2012; Beven  
23  
24 58 and Freer 2001; Jones et al. 2008). Previous work (Ivanov 1981; Taylor 1983) highlights the  
25  
26 59 need for accurate representation of peatland surface flows in particular, to characterise peatland  
27  
28 60 systems effectively. As a result, this approach can provide a powerful means of separating  
29  
30 61 ecological and topographic structures (Hutton and Brazier 2012; Hinsley et al. 2002; Vierling  
31  
32 62 et al. 2008; Chassereau et al. 2011; Clawges et al. 2008; Horning et al. 2010). However, in  
33  
34 63 using these data it is important to note that the applicability of LiDAR is always constrained by  
35  
36 64 the spatial resolution of the processed LiDAR surface (i.e. the resolution of the DSM) and the  
37  
38 65 spatial support (or footprint) of the laser beam itself (Fisher and Tate 2006). Datasets derived  
39  
40 66 from airborne LiDAR are, therefore, subject to implicit (but often unquantified) uncertainty  
41  
42 67 (Aguilar et al. 2010).  
43  
44  
45  
46  
47

48 68 Whilst we acknowledge that LiDAR datasets offer an as yet unparalleled ability to understand  
49  
50 69 landscape structure and function (Korpela et al. 2009; Vierling et al. 2008; Zimble et al. 2003;  
51  
52 70 Evans and Lindsay 2010; Rango et al. 2000), herein we stress the need to better quantify the  
53  
54 71 spatial ( $x$ ,  $y$ ) and vertical ( $z$ ) uncertainty in such data. This would permit an improved  
55  
56 72 interpretation of LiDAR products describing the biotic and abiotic structure of peatlands. One  
57  
58  
59  
60

1  
2  
3 73 way of approaching the problem is to integrate data from other laser scanning technologies  
4  
5 74 operating at finer spatial resolutions (Danson, F. M. et al. 2007), in order to validate the  
6  
7 75 information content of the LiDAR. Here we combine data from a terrestrial laser scanner  
8  
9  
10 76 (TLS) with airborne LiDAR surveys of an upland peatland system in the UK to test the  
11  
12 77 following hypotheses:

- 13  
14  
15 78 1. TLS data can be used to validate the information content of a LiDAR DSM in an  
16  
17 79 upland peatland context, thereby allowing improved spatial characterisation of  
18  
19 80 ecohydrological structures such as above-ground biomass and surface-flow pathways.
- 20  
21 81 2. Airborne LiDAR data allow the discrimination of different ecohydrologically relevant  
22  
23 82 vegetation communities in peatlands.
- 24  
25 83 3. Airborne LiDAR data are capable of detecting the presence and position of  
26  
27 84 anthropogenic landscape features such as drains and archaeological remains which may  
28  
29 85 alter hydrological function in peatlands.

## 30 31 32 33 86 **METHODS**

### 34 35 36 87 *Airborne LiDAR data acquisition and initial processing*

37  
38 88 Airborne LiDAR data were collected by the Environment Agency Geomatics Group (EAGG)  
39  
40 89 (www.geomatics-group.co.uk) in May 2009 at a 0.5 m spatial resolution in the horizontal  
41  
42 90 plane. Two headwater catchments within degraded upland peatland areas in Exmoor National  
43  
44 91 Park, UK were selected to include a wide range of drainage ditch morphology, slope  
45  
46 92 morphology, aspect and vegetation composition. The location of the watershed of these upland  
47  
48 93 catchments (known locally as 'Aclands' [SS 733,384] and 'Spooners' [SS 776,374]) is shown  
49  
50 94 in Figure 1. LiDAR data supplied by EAGG were provided as a 'first return' dataset (0.3 m  
51  
52 95 diameter footprint) and fitted to an even grid of 0.5 × 0.5 m by the data supplier. These data  
53  
54 96 were then processed within a Geographical Information System (GIS; ArcGIS version 9.3.1) to  
55  
56 97 produce a DSM with a cell size equal to 0.5 m. The LiDAR dataset was checked for accuracy  
57  
58  
59  
60

1  
2  
3 98 at 5 separate locations by Geomatics group, using a differential Global Positioning System  
4  
5 99 (DGPS) survey. These ground truth data indicated an average systematic error (or bias) of +  
6  
7 100 0.0004 m and an average random bias of  $\pm 0.047$  m in elevation. The combined RMSE for  
8  
9 101 these data was 0.029 m which was well within the product specification of 0.15 m (personal  
10  
11 102 communication to the author from the EAGG, 2012).

12  
13  
14  
15 103 **#Figure 1 approximately here#**

16  
17  
18 104 ***TLS data collection and processing***

19  
20 105 Ground-based, terrestrial laser scanning (TLS) systems utilise a similar approach to airborne  
21  
22 106 LiDAR, but typically cover smaller extents at finer spatial resolutions. Unlike airborne LiDAR,  
23  
24 107 TLS systems are deployed from one or more fixed locations on the ground surface and have  
25  
26 108 proven useful in providing data describing spatial structural proxies for peatland  
27  
28 109 ecohydrological condition (Anderson et al. 2009; Anderson et al. 2010). Here, TLS data were  
29  
30 110 collected *in situ* using a Leica Geosystems HDS 3000 scanner at the Spooners headwater  
31  
32 111 catchment, in January 2011. The scanner collected ca. 1800 points per second spaced at 0.003  
33  
34 112 m, with a resultant dataset of  $> 7.5 \times 10^6$  points over a spatial extent of  $4.2 \times 10^3$  m<sup>2</sup> in this  
35  
36 113 example. The instrument uses a green laser (wavelength 532 nm), with a beam size of  $< 6$  mm,  
37  
38 114 positional accuracy of  $< 6$  mm and range accuracy of  $< 4$  mm (at a range of  $< 50$  m; Anderson  
39  
40 115 et al. 2009). Data were collected from multiple viewpoints above the peatland surface (Figure  
41  
42 116 2), and were registered into a single point cloud for each site following the method of  
43  
44 117 Anderson et al (2009). Highly visible static stakes were deployed within the survey area to  
45  
46 118 facilitate point-cloud registration; their positions were known to an accuracy of 0.005 m  
47  
48 119 following a DGPS survey. To ensure the scanner had sufficient height above the peatland  
49  
50 120 surface and thus an appropriate angle of incidence to the ground, a flat-bedded tracked vehicle  
51  
52 121 was deployed at each of the scan locations providing a stable elevated platform of a consistent  
53  
54 122 height (ca. 2 m) throughout the survey. The site selected for the survey included three artificial  
55  
56  
57  
58  
59  
60

1  
2  
3 123 drainage ditches measuring approximately 0.3 m × 0.3 m in cross section and was dominated  
4  
5 124 by vegetation typical of the majority of the hill slope area within the catchment. The vegetation  
6  
7 125 included a mixed soft rush (*Juncus effusus*) and purple moor grass (*Molinia caerulea*)  
8  
9 126 dominated sward in which the *M. caerulea* grew in tussock form.

11  
12  
13 127 **#Figure 2 approximately here#**

14  
15 128 A DGPS survey was also used to provide validation transects through the TLS scan areas to  
16  
17 129 provide an independent means of verifying the information content and accuracy of both the  
18  
19 130 TLS and LiDAR datasets during subsequent stages of the analysis. DGPS survey points were  
20  
21 131 taken at 3 – 5 m intervals along a transect and at each location the position of the ground  
22  
23 132 surface and the top of the nearest dense grass tussock structures were recorded, creating pairs  
24  
25 133 of measurements along the transect. The accuracy of the DGPS measurements was ± 0.5 cm in  
26  
27 134 *x*, *y* and ± 2 cm in *z*. The registered TLS point cloud data were imported into Arc GIS 9.3.1. A  
28  
29 135 10 m × 10 m area of interest (AOI) was chosen in an area of dense point cloud coverage and to  
30  
31 136 include a known surface drainage feature.  
32  
33  
34  
35

36 137  
37  
38 138 Subsequent processing aimed to extract the vertical extent of the top of canopy and ground  
39  
40 139 surface respectively. The highest and lowest *z* values within a moving window filter of 0.05  
41  
42 140 m×0.05 m were extracted for the AOI extent and then processed into a 0.01 m discontinuous  
43  
44 141 horizontal grid. A 1 cm grid resolution was chosen to preserve the fine scale variability of the  
45  
46 142 point cloud in the surface generated. To prevent over-representation of outlying cloud points,  
47  
48 143 the resultant data were then aggregated to a grid with a cell size matching the 0.05 m × 0.05 m  
49  
50 144 filter used. Finally, a continuous 0.01 m grid was then interpolated from these data, using the  
51  
52 145 ordinary spherical Kriging method to match the resolution of the discontinuous grid surface.  
53  
54 146 The result was two products - (a) ‘TLSmax’ - the maximum vertical extent (assumed top of  
55  
56 147 canopy) and (b) ‘TLSmin’ – the minimum vertical extent (assumed ground surface). For the  
57  
58  
59  
60



1  
2  
3 148 next stage of processing the same AOI was extracted from the airborne LiDAR data so that the  
4  
5 149 two datasets could be combined.  
6  
7

### 8 ***Combined TLS and LiDAR data analysis*** 9

10 151 In order to address hypothesis one, DSMs generated from both LiDAR and TLS data were  
11  
12 152 compared to understand their information content. A new dataset was derived from the  
13  
14 153 TLSmax, TLSmin and LiDAR data to describe their spatial relationship in three dimensions.  
15  
16 154 Both TLSmax and TLSmin surfaces were classified as either above the height of the LiDAR  
17  
18 155 DSM or below the LiDAR DSM. These classified data were then overlaid on top of a simple  
19  
20 156 hillshade model of both TLSmax and TLSmin to enhance the visual comparison. The  
21  
22 157 percentage of the TLSmax and TLSmin surfaces above and below the LiDAR DSM was then  
23  
24 158 calculated. A transect through both DSMs was plotted alongside the raw TLS point cloud to  
25  
26 159 provide a cross-sectional representation of the relationship between the datasets.  
27  
28  
29  
30

### 31 ***LiDAR analysis to discriminate vegetation and anthropogenic structures*** 32

33 161 To address hypotheses two and three, a model describing the high frequency spatial variation  
34  
35 162 in LiDAR  $z$  (height) was needed. Data were filtered using a 'low pass' moving window ( $11 \times$   
36  
37 163  $11$  pixel neighbourhood) in ERDAS Imagine 2011, resulting in a 'smoothed' surface. These  
38  
39 164 data were subtracted from the original DSM to derive a detrended surface. The low pass  
40  
41 165 window of  $11 \times 11$  pixels was selected to be larger than the maximum patch size of the canopy  
42  
43 166 and microtopographic structure without degrading the signature of the underlying topography.  
44  
45 167 The detrended surface enabled discontinuities in the data to be extracted and classified. For  
46  
47 168 example, step changes that could indicate human activity (e.g. drainage ditches or  
48  
49 169 archaeological remains) (Newman 2010), or areas where the DSM structure changed as a  
50  
51 170 function of shifts in vegetation structure or composition.  
52  
53  
54  
55  
56  
57  
58  
59  
60

1  
2  
3 171 Detrended data derived from the LiDAR DSM were used to identify the  $x, y$  position of  
4  
5 172 microtopographic sinks within the peatland (e.g. tussock/hollow topography or drains). Within  
6  
7 173 the detrended data, sinks were identified automatically by selecting pixels with a height ( $z$ )  
8  
9 174 threshold of -0.11 m. As the  $z$  values in the detrended data represent the height difference from  
10  
11 175 a smoothed surface, negative values highlighted the microtopographic sinks in the landscape,  
12  
13 176 such as drainage features. A  $z$  threshold of -11 cm was chosen on the basis of expert field  
14  
15 177 knowledge of this catchment (this was the minimum depth in the model that could highlight  
16  
17 178 known anthropogenic drainage networks). To analyse the resultant layer further, data were  
18  
19 179 processed to calculate the density of the classified pixels in two dimensional ( $x, y$ ) space. Step  
20  
21 180 changes in the density of these pixels were then used to classify the sinks as being either  
22  
23 181 drainage features or vegetation characteristic of wet flushes.  
24  
25  
26  
27

### 28 182 ***Comparison with hydrological models and vegetation maps***

29  
30  
31 183 Finally, high-resolution aerial photography (2 cm spatial resolution, collected April 2012) was  
32  
33 184 used for the whole Aclands catchment to define the spatial distribution of six distinct  
34  
35 185 vegetation communities based on the species assemblages outlined by Backshall et al. (2001)  
36  
37 186 (wet and dry *Molinia caerulea*, *Juncus* flush, minerotrophic grassland, wet bog, and wet  
38  
39 187 heath). These communities were differentiated using visual changes in canopy structure that  
40  
41 188 were present in the imagery used. These vegetation categories were then manually digitised in  
42  
43 189 order to support interpretation of the RS data analysis under hypothesis two. Although  
44  
45 190 subjective, this technique identified abrupt changes in vegetation at a finer spatial resolution  
46  
47 191 (0.02 m) than the LiDAR DSM (0.5 m) and was therefore considered sufficiently accurate.  
48  
49  
50

51  
52 192 In addition, to support hypothesis three, the raw LiDAR DSM was interrogated with an  
53  
54 193 overland flow accumulation modelling algorithm based on the methods described in Jenson  
55  
56 194 and Domingue (1988). This methodology includes the removal of topographic sinks to ensure  
57  
58  
59  
60

1  
2  
3 195 flow connectivity. The resulting stream network was then classified using the Strahler stream  
4  
5 196 order hierarchy (Strahler 1957). The Jenson and Domingue (1988) model assumes all  
6  
7 197 precipitation becomes runoff and none is lost to interception or groundwater. Although this  
8  
9 198 approach is hydrologically simplified, overland flow is often the predominant discharge from  
10  
11 199 upland peatland systems (Charman 2002; Holden 2005) and therefore this simplicity is  
12  
13 200 scientifically justified and appropriate to describe the hypothetical functioning of surface  
14  
15 201 drainage features in the catchment.  
16  
17

## 18 19 202 **RESULTS**

### 20 203 *Hypothesis one: results of combined TLS and LiDAR analysis*

21  
22  
23 204 To address hypothesis one, the difference between topographic patterns from the TLS and  
24  
25 205 LiDAR data was evaluated. The comparison of TLSmin and TLSmax surfaces to the LiDAR  
26  
27 206 DSM (Figure 3) help to quantify the spatial relationship of TLS and LiDAR data in three  
28  
29 207 dimensions. Most strikingly, the patterning evident in figure 3 illustrates that the linear surface  
30  
31 208 drain feature (highlighted) in the TLSmin surface is almost entirely below the plane of the  
32  
33 209 LiDAR DSM. In the TLSmax surface (3a) almost all of the areas that are lower than the  
34  
35 210 LiDAR DSM correspond with gaps in the vegetation canopy, and are common to both 3a and  
36  
37 211 3b. These locations are visible as shared surface elements and low points in the landscape by  
38  
39 212 both TLSmax and TLSmin. The results in table 1 illustrate that 45% of the TLSmin layer is  
40  
41 213 below the plane of the LiDAR DSM. In contrast, for TLSmax over 87% of the surface is above  
42  
43 214 the plane of the LiDAR DSM. Therefore if TLS data are considered to be 'correct', LiDAR  
44  
45 215 data overestimate the level of the ground surface in 45% of the AOI and underestimate the  
46  
47 216 vegetation canopy in 87% of the AOI.  
48  
49  
50  
51  
52

53  
54 217 **#Figure 3 approximately here#**

55  
56  
57 218 **#Table 1 approximately here#**  
58  
59  
60

1  
2  
3 219 Figure 4 provides more detailed illustration of the relationship between these surfaces along an  
4  
5 220 east – west cross section through the LiDAR and TLS derived DSMs within the AOI. The TLS  
6  
7 221 point cloud exhibits significant vertical variation along this transect with an increased density  
8  
9 222 toward the bottom of its range. The TLSmin surface has an overall trend similar to the LiDAR  
10  
11 223 surface (illustrated in figure 5) although data are more variable than the LiDAR data, falling  
12  
13 224 both above and below the LiDAR DSM in figure 4. Importantly, there is a region (annotated as  
14  
15 225 Drainage Ditch in figure 4) that falls markedly below the plane of the LiDAR data but also  
16  
17 226 corresponds with the position of a drainage ditch in the landscape. In contrast, the TLSmax  
18  
19 227 surface demonstrates a level consistently above the plane of the LiDAR data both as discrete  
20  
21 228 data (figure 4) and as an overall trend (figure5).

22  
23  
24  
25  
26 229 Along this transect, the TLSmax surface also exhibits areas of both high and low variation  
27  
28 230 from the TLSmin surface. In addition, there are six discrete regions in which the TLSmin layer  
29  
30 231 displays increased divergence from the plane of the LiDAR layer (figure 4). These regions also  
31  
32 232 correspond with positions at which the TLSmax surface peaks and the density of the TLS point  
33  
34 233 cloud noticeably decreases. Plotting DGPS points measuring the position of the dense tussock  
35  
36 234 structures and the adjacent ground surface across an extended transect, permits a further test of  
37  
38 235 how well the LiDAR data represents the ground surface (figure 6).

39  
40  
41  
42 236 **#Figure 4 approximately here#**

43  
44  
45 237 **#Figure 5 approximately here#**

46  
47  
48 238 Data in figure 6 confirm that the LiDAR DSM is largely bounded by the surveyed ground  
49  
50 239 surface and the vertical height of the dense tussock structure in this transect. Furthermore, at  
51  
52 240 any DGPS point pair, the LiDAR surface appears skewed toward *either* the ground surface  
53  
54 241 (DGPS tussock bottom) or the tussock tops, with no consistent bias.

1  
2  
3 242 **#Figure 6 approximately here#**  
4  
5

6 243 ***Hypotheses two and three: discrimination of vegetation and anthropogenic structures***  
7

8 244 The extraction of spatially distinct areas of microtopographic sinks from the detrended LiDAR  
9  
10 245 DSM supports evaluation of both hypotheses 2 and 3. In this analysis, dense areas of  
11  
12 246 microtopographic sinks do not fit the expected position of the discrete linear features known to  
13  
14 247 be anthropogenic drainage features. Figure 7 illustrates the results of manually digitising  
15  
16 248 dominant vegetation classes across the catchment (7a) from high-resolution aerial photography  
17  
18 249 (7b) and comparing these with the dense areas of microtopographic sinks classified from  
19  
20 250 detrended LiDAR data from (7c). Visual comparison of the images suggests that the large  
21  
22 251 extents of wet *Molinia caerulea* and wet *Juncus spp.* dominated vegetation observed in the  
23  
24 252 catchment are also captured by the LiDAR data as a complex surface characterised by a high  
25  
26 253 density of microtopographic sinks. The contiguous area that is mapped as wet *Molinia*  
27  
28 254 *caerulea* and wet *Juncus spp.* from aerial photography represents 15.9% of the catchment,  
29  
30 255 versus 18.6% that the LiDAR classification delineates as dominated by vegetation and  
31  
32 256 microtopography characteristic of flushed areas. The smaller (often linear) areas of *Juncus spp.*  
33  
34 257 in the west of the catchment are however, not described well by the LiDAR classification.  
35  
36

37  
38  
39 258 **#Figure 7 approximately here#**  
40  
41

42 259 With respect to hypothesis three, figure 8a reveals that anthropogenic landscape features with  
43  
44 260 constrained vertical variation ( $\geq -0.11$  m) can also be identified and classified using the  
45  
46 261 detrended LiDAR DSM, and the spatial extent of such features delineated and measured. The  
47  
48 262 linear structure of surface drains is visible here as black pixels, alongside the dense areas of  
49  
50 263 microtopographic sinks (blue pixels) used to delineate the flushed (wet *Molinia caerulea* and  
51  
52 264 wet *Juncus spp.* dominated) areas. The linear anthropogenic features extracted using these  
53  
54 265 classifications appear discontinuous across the land surface. Indeed, when the LiDAR DSM is  
55  
56 266 used as an input to simple overland flow routing algorithms (Fig 8b) the anthropogenic  
57  
58  
59  
60

1  
2  
3 267 drainage features extracted (shown as blue lines) demonstrate only a weak control on these  
4  
5 268 flow pathways (grey scale, darker colours representing higher order channels). Many higher  
6  
7 269 order flow accumulation pathways also appear to function entirely independently of the  
8  
9  
10 270 mapped artificial drainage network outlined in blue (Fig 8b), in agreement with the  
11  
12 271 disconnected nature of linear features extracted in fig 8b. The LiDAR data, whilst able to  
13  
14 272 detect the 2D location of drainage ditches, does not therefore appear able to quantify whether  
15  
16 273 or not they are continuous drainage features in the landscape.

17  
18  
19 274 **#Figure 8 approximately here#**

## 20 21 275 **DISCUSSION**

22  
23  
24 276 Moving beyond qualitative visual analysis of LiDAR data, such as simple hillshade models, is  
25  
26 277 an essential step to quantify landscape scale ecohydrological functioning and the associated  
27  
28 278 landscape services. Given this, understanding the accuracy with which LiDAR products are  
29  
30 279 able to measure ecohydrologically-relevant structures in the uplands is critical if such analysis  
31  
32 280 is to be considered representative of “real world” structure and subsequent function. This study  
33  
34 281 has shown that while vegetation canopy height and drainage ditch depth are underestimated by  
35  
36 282 airborne LiDAR DSMs, the aerial extent of these features can still be determined in a spatial  
37  
38 283 context. The following sections discuss the various ramifications of these findings.

### 39 40 41 42 284 *Vertical accuracy of LiDAR Data – combined LiDAR and TLS analysis*

43  
44  
45 285 Hypothesis one explored how airborne LiDAR DSMs compare with TLS data, in relation to  
46  
47 286 their abilities to capture structural information about vegetation and topography. Numerous  
48  
49 287 researchers have alluded to the sources of error in a wide range of DSM’s (Fisher and Tate  
50  
51 288 2006; Li et al. 2011; Wise 2011). However, few authors propose solutions to resolve levels of  
52  
53 289 error with respect to independent measurements (see Aguilar et al. 2010 and Hodgson and  
54  
55 290 Bresnahan 2004 for notable exceptions). Herein, we illustrate that the TLSmax and TLSmin

1  
2  
3 291 surfaces describe the maximum and minimum measured vertical extent of the vegetation  
4  
5 292 canopy at a fine spatial resolution. Therefore, TLS data are extremely useful in describing the  
6  
7 293 information content and error associated with airborne LiDAR data and its ability to describe  
8  
9 294 spatial shifts in vegetation organisation. Data presented in figure 3 illustrate that the LiDAR  
10  
11 295 DSM elevation values correlate with the TLSmin surface far more than they do with the  
12  
13 296 TLSmax surface over the extent of the AOI (87% of TLSmax is above the plane of the LiDAR  
14  
15  
16 297 data). These results demonstrate that the LiDAR data most closely represent the ground surface  
17  
18 298 and not the canopy structure. Furthermore, the highlighted surface drain feature (figure 3) is  
19  
20 299 entirely below the plane of the LiDAR DSM in the AOI studied. Such underestimation of  
21  
22 300 vegetation canopy heights and the depth of drainage features have important implications  
23  
24 301 where LiDAR-derived structures are used as indicators of ecohydrological condition (Anderson  
25  
26 302 et al. 2010), and as inputs to spatially distributed models (Beven, 2011).

27  
28  
29  
30 303 More detailed analysis of the magnitude of vertical variation between the LiDAR and TLS  
31  
32 304 layers (figures 4 and 5) also illustrated that the LiDAR DSM more closely represents a  
33  
34 305 smoothed version of the ground surface (described by the TLSmin data) lacking  
35  
36 306 microtopographic structure. Topographic features, such as the surface drainage network, are  
37  
38 307 estimated in error in DSM data for the following reasons according to Fisher and Tate (2006):

- 39  
40  
41  
42 308 • Variability in the accuracy, density and distribution of source data,  
43  
44 309 • Processing and interpolation  
45  
46 310 • Characteristics of the terrain surface being modelled.

47  
48  
49  
50 311 In this case the LiDAR DSMs created provide one  $x$ ,  $y$ ,  $z$  coordinate for every 0.5 m cell, which  
51  
52 312 is a relatively coarse resolution when compared with the scale of drainage ditch features (often  
53  
54 313 they are only 0.3 m wide in these landscapes). In addition, the dense, low-sward vegetation  
55  
56 314 tussocks disrupt the return of the laser pulse from the ground surface such that

1  
2  
3 315 microtopographic depressions are not captured consistently, especially when tussock forming  
4  
5 316 grasses occur within, or overhang, surface drainage pathways (as evident in figure 3).  
6  
7 317 Therefore, in contrast to forested landscapes, where vegetation is typically less dense and more  
8  
9 318 uniform in height (Vierling et al 2008), it is likely that LiDAR DSMs will always generate an  
10  
11 319 uncertain representation of the ecosystem structure in short-sward ecosystems. In this example,  
12  
13 320 the LiDAR DSM is biased towards the ground surface, as delineated by the TLSmin dataset,  
14  
15 321 which lies consistently close to and above the trend line for the LiDAR DSM (figure 5).  
16  
17

18  
19 322 To understand the specific effect of denser vegetation components on the LiDAR DSM, DGPS  
20  
21 323 survey data were also compared with the LiDAR surface. Figure 6 illustrated that the LiDAR  
22  
23 324 DSM data captured the ground surface *and* dense grass tussock centres reasonably well as a  
24  
25 325 composite surface, with all points falling within the bounds created from the DGPS  
26  
27 326 measurements. This additional data analysis suggests that the LiDAR DSM data represent both  
28  
29 327 the ground surface and the denser components of the vegetation structure *only* and not the  
30  
31 328 sward canopy structure. For an airborne product flown at an altitude of 800 – 1000m above  
32  
33 329 ground level, this ability to approximate the range of tussock top-bottom values suggests some  
34  
35 330 promise in using the LiDAR DSM in these low-sward landscapes to assess habitat structure  
36  
37 331 (Anderson et al. 2010; Korpela et al. 2009; Vierling et al. 2008). However, these results  
38  
39 332 highlight the necessity to evaluate the modelled LiDAR surface with finer resolution data prior  
40  
41 333 to inference of ecohydrological structure. Indeed, where LiDAR data are used to provide  
42  
43 334 metrics of habitat condition without three-dimensional validation of observed vegetation  
44  
45 335 structures such as TLS (Kincey and Challis 2009; Korpela et al. 2009; Li et al. 2011; Streutker  
46  
47 336 and Glenn 2006), the certainty with which we can use LiDAR data to understand the condition  
48  
49 337 of these systems spatially is limited.  
50  
51  
52  
53

54  
55  
56 338 TLS data in isolation also provide a useful tool in the quantification of both the ecological and  
57  
58 339 hydrological structure of these upland ecosystems over smaller extents. The technique  
59  
60



1  
2  
3 340 presented here provides discrete layers which are useful in measuring vegetation  
4  
5 341 canopy/biomass and the underlying surface structure. Whether used independently or in  
6  
7 342 conjunction with airborne LiDAR, critical evaluation of TLS data is still necessary to ensure  
8  
9 343 robust interpretation. For example, data presented here (figure 4) illustrate that at locations  
10  
11 344 where the point cloud becomes sparse the TLSmin layer appears to offer a markedly poorer  
12  
13 345 representation of the underlying ground surface. In agreement with wider studies using TLS  
14  
15 346 (Anderson et al. 2009; Watt and Donoghue 2005), these findings highlight the difficulties of  
16  
17 347 using TLS data to measure complex and fine-scaled vegetation structure in situ. In this case,  
18  
19 348 the error is attributable to the method of data generation (Fisher and Tate 2006). i.e. vegetation  
20  
21 349 canopy completely obscuring the ground from the laser or because the area is subject to  
22  
23 350 shadowing in the point cloud. As such, this deviation of the TLSmin surface from the LiDAR  
24  
25 351 DSM agrees with the LiDAR data predominantly describing a smoothed ground surface.  
26  
27 352 However, these results illustrate that structural measurements from any platform, even at fine  
28  
29 353 spatial scales, can be subject to the same sources of error in short sward ecosystem.

#### 354 ***Discrimination of vegetation and anthropogenic structures***

355 Although the preceding results and discussion demonstrate that LiDAR data underestimate  
36  
37 356 both canopy height and drainage network volume, numerical interrogation of detrended LiDAR  
38  
39 357 data has shown that spatial information on ecohydrologically relevant vegetation communities  
40  
41 358 (hypothesis 2) and anthropogenic drainage features (hypothesis 3), can still be captured. Data  
42  
43 359 in figure 7 confirm that the detrended LiDAR data can be used to effectively map the extent of  
44  
45 360 flushed (i.e. wetter) vegetation communities. However, the preceding findings suggest that  
46  
47 361 increased surface complexity used to delineate these areas is, in fact, a measurement of the  
48  
49 362 change in the sub-canopy, highlighting microtopographic landforms associated with these  
50  
51 363 waterlogged vegetation communities dominated by *Juncus* spp. and wet *Molinia caerulea*  
52  
53 364 stands.  
54  
55  
56  
57  
58  
59  
60

1  
2  
3 365 Features identified as anthropogenic peatland surface drainage in this analysis have been  
4  
5 366 validated as being (largely) continuous and connected, following extensive fieldwork and GPS  
6  
7 367 mapping of drainage features at these sites (figure 8). However, results in figure 8 suggest that  
8  
9  
10 368 they appear to be highly discontinuous features when detected by LiDAR. Under-  
11  
12 369 representation of microtopographic structure in LiDAR DSMs (figure 4) explains why such  
13  
14 370 drainage features extracted for the Aclands catchment in figure 8a appear to be discontinuous.  
15  
16 371 Consequently, these features are shown to have only a limited influence on the flow paths  
17  
18 372 modelled in the flow accumulation model illustrated in figure 8b, though in reality, they may  
19  
20  
21 373 be highly significant in controlling surface-flow networks. The extent to which such LiDAR  
22  
23 374 data can be relied upon as good representations of microtopography (anthropogenic or  
24  
25 375 otherwise) controlling ecohydrological function, is therefore subject to the same implicit error  
26  
27 376 or uncertainty previously discussed (Jones et al. 2008). Where such data are used as inputs to  
28  
29 377 numerical hydrological models in peatland landscapes (Rothwell et al. 2010), understanding  
30  
31 378 such uncertainty in the representation of drainage structure is critical to ensure the spatial  
32  
33 379 quality of model predictions.

34  
35  
36  
37 380 Acknowledging the error and understanding the source of it in such data can also be  
38  
39 381 advantageous to the ecohydrologist. Knowing the nature of the error and its magnitude makes  
40  
41 382 airborne LiDAR data potentially far more powerful as inputs to ecohydrological modelling  
42  
43  
44 383 frameworks. For example, using numerical processing such as “growing” extracted features  
45  
46 384 (Espindola et al. 2006) describing discontinuous drainage features and using these to modify  
47  
48 385 DSM values (Li et al. 2011) may allow researchers to represent the connectivity of surface  
49  
50 386 drainage structures in a modelled catchment more accurately. Subsequently, better predictions  
51  
52 387 of both the spatial distribution of flow routing and resultant downstream hydrographs may  
53  
54 388 result, in turn aiding the quantification of the associated ecohydrological landscape services  
55  
56  
57 389 (Grand-Clement et al. 2013). These data also highlight the value of a combined RS approach in  
58  
59  
60

1  
2  
3 390 confirming assumptions made from any one dataset. For example, cross validation of modelled  
4  
5 391 surface wetness indices generated from LiDAR and TABI (airborne thermography data),  
6  
7 392 (Luscombe et al. 2012) or LiDAR and near infra-red data (Harris and Bryant 2009) can be  
8  
9  
10 393 performed, enabling the observed ecohydrological patterning to be evaluated prior to  
11  
12 394 integration into numerical modelling of the ecohydrological functioning.

## 13 14 15 395 **CONCLUSION**

16  
17 396 This paper demonstrates that the spatially explicit measurements provided by LiDAR datasets  
18  
19 397 are subject certain to specific errors, related to both the spatial resolution of the dataset and the  
20  
21 398 interaction of laser ranging systems with short-sward landscapes. Results show that airborne  
22  
23 399 LiDAR data underestimate vegetation canopy volume/height and the volume/depth of surface  
24  
25 400 drainage networks, both of which are key spatial variables in understanding ecohydrological  
26  
27 401 functioning at a landscape scale. Understanding this uncertainty improves the way in which  
28  
29 402 these data can be used as numerical model inputs, and the confidence which researchers should  
30  
31 403 place on these data when used as a surrogate for field measurements over a variety of  
32  
33 404 disciplines and ecosystems. Furthermore, this work demonstrates that using TLS data, the  
34  
35 405 canopy structure *can* be described at a fine spatial resolution and with greater precision than  
36  
37 406 with LiDAR data, although over far smaller extents. These data illustrate the need to couple  
38  
39 407 LiDAR data with fine spatial resolution altimetry data (i.e. TLS) and field measurements, to  
40  
41 408 improve models of the ecosystem structure and describe the spatial attributes of the ecosystem  
42  
43 409 at a scale that is appropriate to capture the ecohydrological functioning of the landscape.  
44  
45  
46  
47  
48  
49 410

1  
2  
3 411 **References**4  
5 4126  
7 413 Aguilar FJ, Mills JP, Delgado J, Aguilar MA, Negreiros JG, Perez JL. 2010. Modelling vertical  
8 414 error in LiDAR-derived digital elevation models. *ISPRS Journal of Photogrammetry and*  
9 415 *Remote Sensing* **65(1)** : 103-110.  
10  
11

12 416

13  
14 417 Anderson K, Bennie J, Wetherelt A. 2009. Laser scanning of fine scale pattern along a  
15 418 hydrological gradient in a peatland ecosystem. *Landscape Ecology* **25(3)** : 477-492.  
16  
17

18 419

19 420 Anderson K, Bennie J, Milton EJ, Hughes PDM, Lindsay R, Meade R. 2010. Combining  
20 421 LiDAR And Ikonos Data For Eco-hydrological Classification Of An Ombrotrophic Peatland.  
21 422 *Journal of Environmental Quality*. **39(1)** : 260-273.  
22  
23

24 423

25  
26 424 Backshall J, Manley J, Rebane M. 2001. *The Upland Management Handbook*. English Nature.  
27  
28

29 425

30 426 Bain CG, Bonn A, Stoneman R, Chapman S, Coupar A, Evans M, Gearey B, Howat M,  
31 427 Joosten H, Keenleyside C, Labadz J, Lindsay R, Littlewood N, Lunt P, Miller CJ, Moxey A,  
32 428 Orr H, Reed M, Smith P, Swales V, Thompson D.B.A, Thompson P.S, Van de Noort R,  
33 429 Wilson JD, Worrall F. 2011. *IUCN UK Commission of Inquiry on Peatlands*. IUCN UK  
34 430 Peatland Programme: Edinburgh.  
35  
36

37 431

38  
39 432 Barber KE. 1981. *Peat Stratigraphy and Climatic Change*. Rotterdam : Balkema.  
40  
41

42 433

43 434 Barbier N, Proisy C, Vega C, Sabatier D, Couteron P. 2011. Bidirectional texture function of  
44 435 high resolution optical images of tropical forest: An approach using LiDAR hillshade  
45 436 simulations. *Remote Sensing of Environment* **115(1)** : 167-179.  
46  
47

48 437

49 438 Belyea LR, Clymo RS. 2001. Feedback control of the rate of peat formation. *Proceedings of*  
50 439 *the Royal Society of London: Biological Sciences* **268** : 1315 - 1321.  
51  
52

53 440

54 441 Beven K. 2012. *Rainfall-Runoff Modelling, The Primer*. John Wiley & Sons Ltd: Chichester.  
55  
56

57 442

58 443 Beven K, Freer J. 2001. A dynamic TOPMODEL. *Hydrological Processes* **15(10)** : 1993-2011.  
59  
60

- 1  
2  
3 444  
4 445 Charman D. 2002. *Peatlands and Environmental Change*. John Wiley & Sons Ltd: Chichester.  
5  
6 446  
7  
8 447 Chassereau JE, Bell JM, Torres R. 2011. A comparison of GPS and LiDAR salt marsh DEMs.  
9  
10 448 *Earth Surface Processes and Landforms* **36(13)** : 1770-1775.  
11 449  
12  
13 450 Clawges R, Vierling K, Vierling L, Rowell E. 2008. The use of airborne lidar to assess avian  
14 451 species diversity, density, and occurrence in a pine/aspen forest. *Remote Sensing of*  
15 452 *Environment* **112(5)** : 2064-2073.  
16  
17 453  
18  
19 454 Danson FM, Hetherington D, Morsdorf F, Koetz B, Allgower B. 2007. "Forest Canopy Gap  
20 455 Fraction From Terrestrial Laser Scanning." *Geoscience and Remote Sensing Letters*, IEEE **4(1)**  
21 : 157-160.  
22  
23 456  
24  
25 457  
26 458 Drewitt AL, Manley VJ. 1997. *The vegetation of the mountains and moorlands of England*.  
27 English Nature Research Reports. English Nature, pp. 218.  
28 459  
29 460  
30  
31 461 Emanuel RE, Hazen AG, McGlynn BL, Jencso KG. 2013. Vegetation and topographic  
32 462 influences on the connectivity of shallow groundwater between hillslopes and streams.  
33 463 *Ecohydrology* **7** : 887-895. DOI: 10.1002/eco.1409  
34  
35 464  
36  
37 465 Espindola GM, Camara G, Reis IA, Bins LS, Monteiro AM. 2006. Parameter selection for  
38 466 region growing image segmentation algorithms using spatial autocorrelation. *International*  
39 467 *Journal of Remote Sensing* **27(14)** : 3035-3040.  
40  
41 468  
42  
43 469 Evans M, Lindsay J. 2010. High resolution quantification of gully erosion in upland peatlands  
44 470 at the landscape scale. *Earth Surface Processes and Landforms* **35(8)** : 876-886.  
45  
46 471  
47  
48 472 Fisher B, Turner RK, Morling P. 2009. Defining and classifying ecosystem services for  
49 473 decision making. *Ecological Economics* **68(3)** : 643-653.  
50  
51 474  
52  
53 475 Fisher PF, Tate NJ. 2006. Causes and consequences of error in digital elevation models.  
54 476 *Progress in Physical Geography* **30(4)** : 467-489.  
55  
56 477  
57  
58  
59  
60

- 1  
2  
3 478 Grand-Clement E, Anderson K, Smith D, Luscombe DJ, Gatis N, Ross M, Brazier RE. 2013.  
4 479 Evaluating ecosystem goods and services after restoration of marginal upland peatlands in  
5 480 South-West England. *Journal of Applied Ecology* **50(2)** : 324-334.  
6  
7 481  
8  
9 482 Harris A, Bryant RG. 2009. A multi-scale remote sensing approach for monitoring northern  
10 483 peatland hydrology: Present possibilities and future challenges. *Journal of Environmental*  
11 484 *Management* **90(7)** : 2178-2188.  
12  
13 485  
14  
15 486 Hinsley SA, Hill RA, Gaveau DLA, Bellamy PE. 2002. Quantifying woodland structure and  
16 487 habitat quality for birds using airborne laser scanning. *Functional Ecology* **16(6)** : 851-857.  
17  
18 488  
19 489 Hodgson ME, Bresnahan P. 2004. Accuracy of airborne lidar-derived elevation: empirical  
20 490 assessment and error budget. *Photogrammetric Engineering and Remote Sensing* **70(3)** : 331-  
21 491 340.  
22  
23 492  
24  
25 493 Holden J, Chapman PJ, Labadz JC. 2004. Artificial drainage of peatlands: hydrological and  
26 494 hydrochemical process and wetland restoration. *Progress in Physical Geography* **28(1)** : 95-  
27 495 123.  
28  
29 496  
30 497 Holden, J. 2005. Peatland hydrology and carbon release: why small-scale process matters.  
31 498 *Philosophical Transactions of the Royal Society a-Mathematical Physical and Engineering*  
32 499 *Sciences* **363** : 2891-2913.  
33  
34 500  
35  
36 501 Horning N, Robinson JA, Sterling EJ, Turner W, Spector S (eds). 2010. *Remote Sensing for*  
37 502 *Ecology and Conservation: A Handbook of Techniques*. Oxford University Press: Oxford and  
38 503 New York.  
39  
40 504  
41  
42 505 Hutton C, Brazier RE. 2012. Quantifying riparian zone structure from airborne LiDAR:  
43 506 Vegetation filtering, anisotropic interpolation, and uncertainty propagation. *Journal of*  
44 507 *Hydrology* **442-443(0)** : 36-45.  
45  
46 508  
47  
48 509 Ivanov KE. 1981. *Water movement in mirelands*. Academic Press Inc: London.  
49  
50 510  
51  
52  
53  
54  
55  
56  
57  
58  
59  
60

1  
2  
3 511 Jenson SK, Domingue JO. 1988. Extracting topographic structure from digital elevation data  
4 512 for geographic information system analysis. *Photogrammetric Engineering and Remote*  
5 513 *Sensing* **54(11)** : 1593-1600.

6  
7  
8 514

9  
10 515 Jones KL, Poole GC, O'Daniel SJ, Mertes LAK, Stanford JA. 2008. Surface hydrology of low-  
11 516 relief landscapes: Assessing surface water flow impedance using LIDAR-derived digital  
12 517 elevation models. *Remote Sensing of Environment* **112(11)** : 4148-4158.

13  
14  
15 518

16 519 Kinsey M, Challis K. 2009. Monitoring fragile upland landscapes: The application of airborne  
17 520 lidar. *Journal for Nature Conservation* **18(2)** : 126-134.

18  
19  
20 521

21 522 Korpela I, Koskinen M, Vasander H, Holopainen M, Minkkinen K. 2009. Airborne small-  
22 523 footprint discrete-return LiDAR data in the assessment of boreal mire surface patterns,  
23 524 vegetation, and habitats. *Forest Ecology and Management* **258(7)** : 1549-1566.

24  
25  
26 525

27  
28 526 Lane C, D'Amico E. 2010. calculating the ecosystem service of water storage in isolated  
29 527 wetlands using LiDAR in north central Florida, USA. *Wetlands* **30(5)** : 967-977.

30  
31  
32 528

33 529 Li S, MacMillan RA, Lobb DA, McConkey BG, Moulin A, Fraser WR. 2011. Lidar DEM  
34 530 error analyses and topographic depression identification in a hummocky landscape in the  
35 531 prairie region of Canada. *Geomorphology* **129(3-4)** : 263-275.

36  
37  
38 532

39 533 Lindsay R. 2010. *Peatbogs and Carbon: A Critical Synthesis*. University of East London:  
40 534 London.

41  
42  
43 535

44 536 Luscombe DJ, Anderson K, Grand-Clement E, Le-Feuvre N, Smith D, & Brazier RE. 2012.  
45 537 April. Assessing the ecohydrological status of a drained peatland: Combining thermal airborne  
46 538 imaging, laser scanning technologies and ground water monitoring. *EGU General Assembly*  
47 539 *Conference Abstracts* (Vol. 14, p. 740).

48  
49  
50  
51 540

52  
53 541 Mitchell PJ, Lane PNJ, Benyon RG. 2012. Capturing within catchment variation in  
54 542 evapotranspiration from montane forests using LiDAR canopy profiles with measured and  
55 543 modelled fluxes of water. *Ecohydrology* **5(6)** : 708-720.

56  
57  
58 544

- 1  
2  
3 545 Moore PD, Bellamy DJ. 1974. *Peatlands*. London : Elek Science.  
4  
5 546  
6 547 Newman P. (2010). Domestic and industrial peat cutting on North-Western Dartmoor,  
7  
8 548 Devonshire. An archaeological and historical investigation. In. South-West landscape  
9  
10 549 Investigations reports, Dartmoor National Park.  
11  
12 550  
13 551 Rango A, Chopping M, Ritchie J, Havstad K, Kustas W, Schmugge T. 2000. morphological  
14  
15 552 characteristics of shrub coppice dunes in desert grasslands of southern new mexico derived  
16  
17 553 from scanning LIDAR. *Remote Sensing of Environment* **74(1)** : 26-44.  
18  
19 554  
20 555 Rothwell JJ, Lindsay JB, Evans MG, Allott THE. 2010. Modelling suspended sediment lead  
21  
22 556 concentrations in contaminated peatland catchments using digital terrain analysis. *Ecological*  
23  
24 557 *Engineering* **36(5)** : 623-630.  
25  
26 558  
27 559 Strahler AN. 1957. Quantitative analysis of watershed geomorphology. *American Geophysical*  
28  
29 560 *Union Transactions* **38(6)** : 912-920.  
30  
31 561  
32 562 Streutker DR, Glenn NF. 2006. LiDAR measurement of sagebrush steppe vegetation heights.  
33  
34 563 *Remote Sensing of Environment* **102(1)** : 135-145.  
35  
36 564  
37 565 Taylor J. 1983. Peatlands of Great Britain and Ireland. In: *Mires: Swamp, Bog, Fen and Moor.*  
38  
39 566 *4B Regional Studies (Ecosystems of the World)* ed. Gore AJP. pp. 1-46. Elsevier Scientific:  
40  
41 567 Amsterdam.  
42  
43 568  
44 569 Turnbull L, Wainwright J, Brazier RE. 2008. A conceptual framework for understanding semi-  
45  
46 570 arid land degradation: ecohydrological interactions across multiple-space and time scales.  
47  
48 571 *Ecohydrology* **1(1)** : 23-34.  
49  
50 572  
51 573 Vierling KT, Vierling LA, Gould WA, Martinuzzi S, Clawges RM. 2008. LiDAR: shedding  
52  
53 574 new light on habitat characterization and modeling. *Frontiers in Ecology and the Environment*  
54  
55 575 **6(2)** : 90-98.  
56  
57 576  
58 577 Watt PJ, Donoghue DNM. 2005. Measuring forest structure with terrestrial laser scanning.  
59  
60 578 *International Journal of Remote Sensing* **26(7)** : 1437-1446.



1  
2  
3 579

4 580 Wise S. 2011. Cross-validation as a means of investigating DEM interpolation error.  
5  
6 581 *Computers & Geosciences* **37(8)** : 978-991.  
7

8 582

9  
10 583 Zimble DA, Evans DL, Carlson GC, Parker RC, Grado SC, Gerard PD. 2003. Characterizing  
11 584 vertical forest structure using small-footprint airborne LiDAR. *Remote Sensing of Environment*  
12  
13 585 **87(2-3)** : 171-182.  
14

15  
16 586  
17  
18  
19  
20  
21  
22  
23  
24  
25  
26  
27  
28  
29  
30  
31  
32  
33  
34  
35  
36  
37  
38  
39  
40  
41  
42  
43  
44  
45  
46  
47  
48  
49  
50  
51  
52  
53  
54  
55  
56  
57  
58  
59  
60

For Peer Review

587 **Tables**

588

589 **Table 1**, Percentage of the TLSmax and TLSmin layers that have z values above

590 and below the plane of the LiDAR derived DSM.

<b>Classification</b>	<b>TLS Max Surface</b>	<b>TLS Min Surface</b>
% below LiDAR DSM	13	45
% above LiDAR DSM	87	55

591

592

Peer Review

1  
2  
3 593 **Figure captions**  
4 594

5  
6 595 **Figure 1:** a) and b) Location of Aclands and Spooners study catchments and c) the  
7  
8 596 TLS study area within Spooners watershed defined from airborne LiDAR data. d)  
9  
10 597 and e) illustrate the study area used for the TLS survey. d) Shows the scan locations  
11  
12 598 and AOI overlaying an aerial photograph of the study area (Co-ordinates for upper  
13  
14 599 left  $51^{\circ} 7'23.81''\text{N}$ ,  $3^{\circ}45'2.76''\text{W}$  and bottom right  $51^{\circ} 7'21.69''\text{N}$ ,  $3^{\circ}44'59.70''\text{W}$ ). e)  
15  
16 600 Shows the spatial extent of the TLS data collected as a grid, each dot representing  
17  
18 601 one of  $> 7.5 \times 10^6$  data points.  
19  
20  
21  
22  
23

24 602 **Figure 2:** TLS data capture locations and respective overlapping scan zones. The  
25  
26 603 darker polygon within the station 4 scan region represents the area of greatest point  
27  
28 604 cloud overlap as shown in figure 1e). The Area of Interest (AOI) is indicated,  
29  
30 605 showing that it lies within the zone of maximal point-cloud overlap.  
31  
32  
33  
34  
35

36 606 **Figure 3:** Hillshade models of both (a) TLSmax and (b) TLSmin Surfaces for the  
37  
38 607 Area of Interest (AOI). Areas higher than the LiDAR DSM surface are overlain with  
39  
40 608 black and those below the LiDAR DSM are overlain with white.  
41  
42  
43  
44

45 609 **Figure 4:** TLS and LiDAR topographic profiles extracted from the Studied AOI  
46  
47 610 within Spooners Catchment. TLSmax and TLSmin represent the maximum and  
48  
49 611 minimum vertical extent of the TLS data along this transect. Annotations highlight  
50  
51 612 the position of the drainage ditch in the transect and an example of a location where  
52  
53 613 TLSmin and LiDAR surfaces diverge as a result of a sparser point cloud density.  
54  
55  
56  
57  
58  
59  
60

1  
2  
3 614 **Figure 5:** Modelled relationships (second order polynomial,  $N = 1040$  for TLSmax  
4  
5 615 and TLSmin) describing the under-representation of the vegetation canopy  
6  
7 616 (TLSmax) by LiDAR DSM data. Data are generated as trends of topographic  
8  
9 617 profiles extracted in figure 4.

11  
12  
13  
14 618 **Figure 6:** Alternate LiDAR topographic profile extracted from the wider TLS scan  
15  
16 619 zone (figure 1) within Spooners catchment. DGPS Survey data describing the  
17  
18 620 maximum and minimum vertical extent of dense vegetation components (tussocks)  
19  
20 621 are included as paired measurements along the transect length.

21  
22  
23  
24  
25  
26 622 **Figure 7:** Habitat mapping of Aclands Catchment. (a) Vegetation communities  
27  
28 623 digitised from aerial imagery. (b) High resolution aerial photograph. (c) Flushed  
29  
30 624 vegetation Area delineated from classified LiDAR data.

31  
32  
33  
34  
35 625 **Figure 8:** Mapping of surface drainage. (a) Data extracted from detrended LiDAR  
36  
37 626 data (Aclands Catchment) and classified into surface drainage networks, whether  
38  
39 627 natural or artificial (Black pixels) and rush dominated “flushed” zones (blue  
40  
41 628 pixels). Pixels were classified using a threshold of pixel density. (b) A simple  
42  
43 629 overland flow accumulation model with streams ordered using the Strahler  
44  
45 630 classification (Strahler 1957) whereby stream size is classified according to a  
46  
47 631 hierarchy of tributaries. A stream with no tributaries is 1st order; when two 1st  
48  
49 632 order streams meet they subsequently form a 2nd order stream and so on. Only 4th  
50  
51 633 to 9th order streams are displayed.

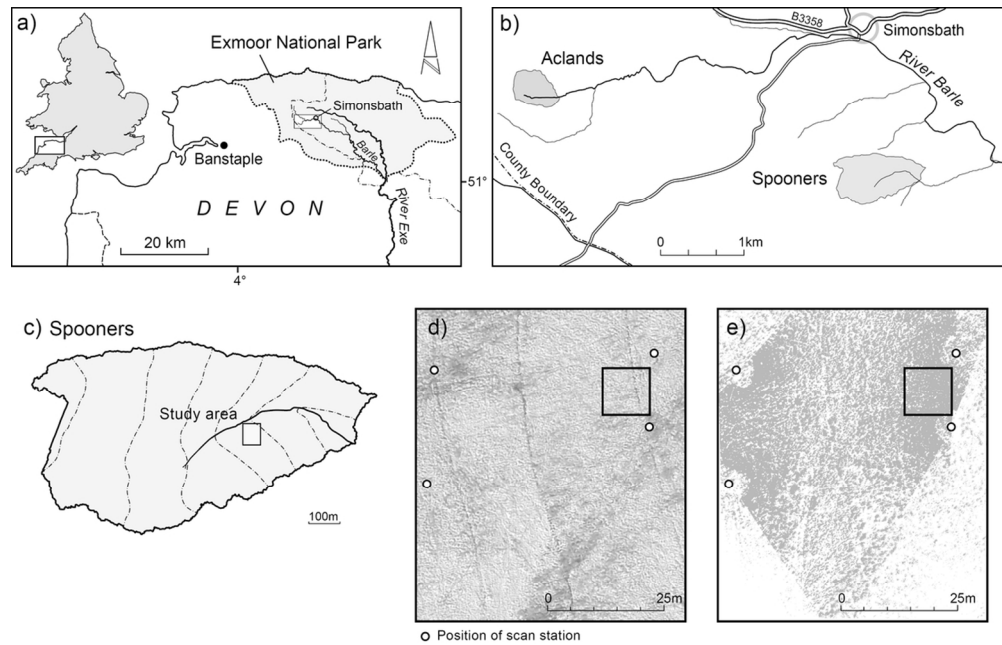


Figure 1: a) and b) Location of Aclands and Spooners study catchments and c) the TLS study area within Spooners watershed defined from airborne LiDAR data. d) and e) illustrate the study area used for the TLS survey. d) Shows the scan locations and AOI overlaying an aerial photograph of the study area (Coordinates for upper left  $51^{\circ} 7'23.81''N$ ,  $3^{\circ}45'2.76''W$  and bottom right  $51^{\circ} 7'21.69''N$ ,  $3^{\circ}44'59.70''W$ ). e) Shows the spatial extent of the TLS data collected as a grid, each dot representing one of  $> 7.5 \times 10^6$  data points.

107x72mm (300 x 300 DPI)

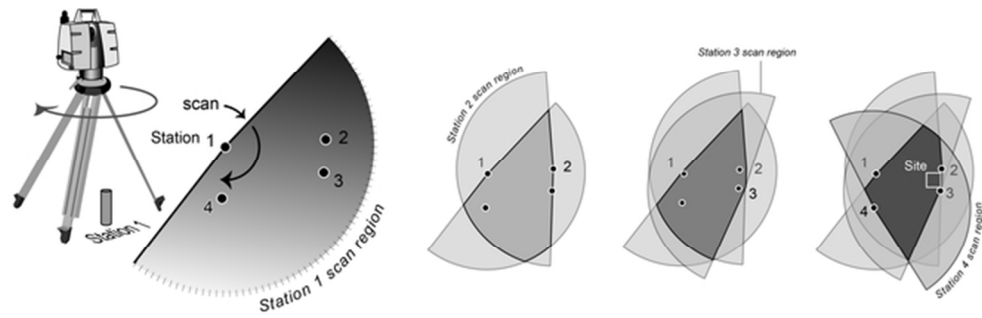


Figure 2: TLS data capture locations and respective overlapping scan zones. The darker polygon within the station 4 scan region represents the area of greatest point cloud overlap as shown in figure 1e). The Area of Interest (AOI) is indicated, showing that it lies within the zone of maximal point-cloud overlap.  
57x20mm (300 x 300 DPI)

Peer Review

1  
2  
3  
4  
5  
6  
7  
8  
9  
10  
11  
12  
13  
14  
15  
16  
17  
18  
19  
20  
21  
22  
23  
24  
25  
26  
27  
28  
29  
30  
31  
32  
33  
34  
35  
36  
37  
38  
39  
40  
41  
42  
43  
44  
45  
46  
47  
48  
49  
50  
51  
52  
53  
54  
55  
56  
57  
58  
59  
60

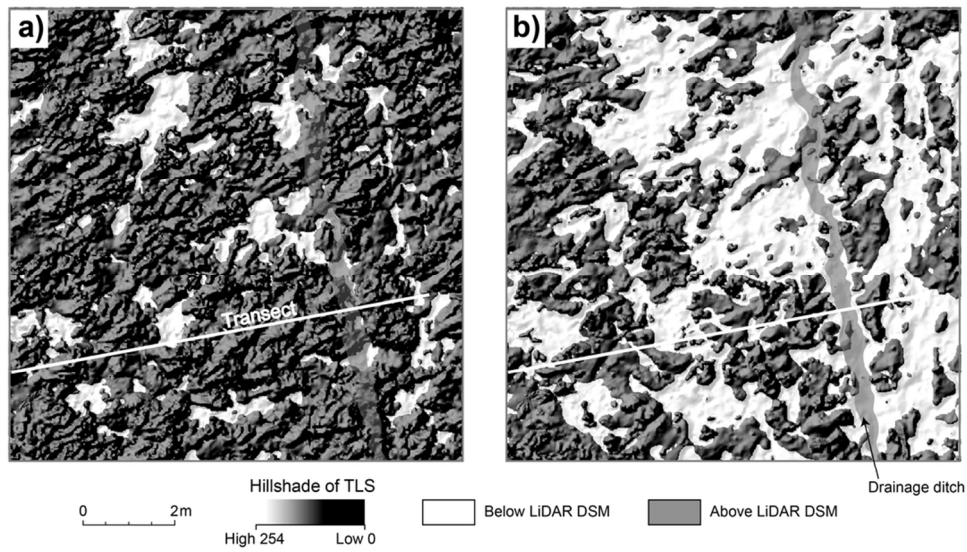


Figure 3: Hillshade models of both (a) TLSmax and (b) TLSmin Surfaces for the Area of Interest (AOI). Areas higher than the LiDAR DSM surface are overlain with black and those below the LiDAR DSM are overlain with white.  
94x54mm (300 x 300 DPI)

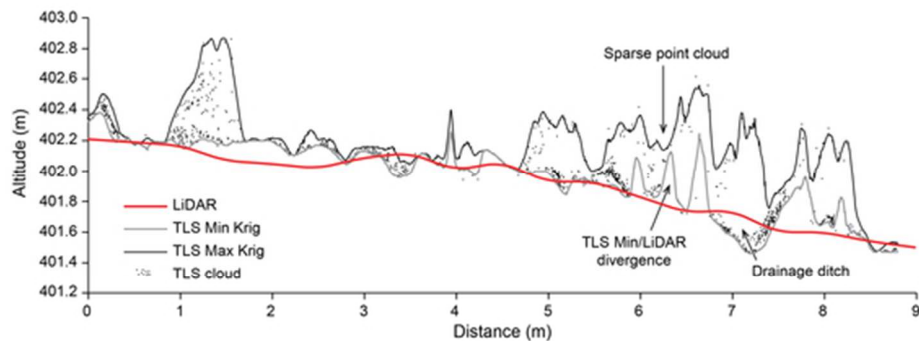


Figure 4: TLS and LiDAR topographic profiles extracted from the Studied AOI within Spooners Catchment. TLSmax and TLSmin represent the maximum and minimum vertical extent of the TLS data along this transect. Annotations highlight the position of the drainage ditch in the transect and an example of a location where TLSmin and LiDAR surfaces diverge as a result of a sparser point cloud density.  
52x21mm (300 x 300 DPI)



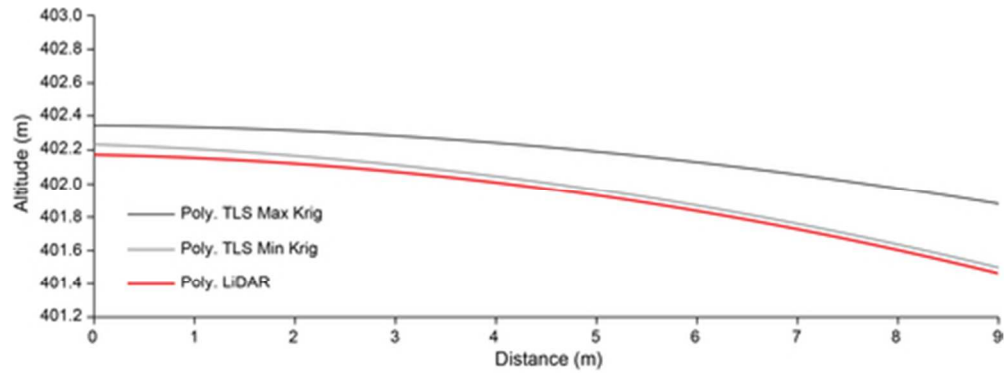


Figure 5: Modelled relationships (second order polynomial, N =1040 for TLSmax and TLSmin) describing the under-representation of the vegetation canopy (TLSmax) by LiDAR DSM data. Data are generated as trends of topographic profiles extracted in figure 4.  
41x15mm (300 x 300 DPI)

Peer Review

1  
2  
3  
4  
5  
6  
7  
8  
9  
10  
11  
12  
13  
14  
15  
16  
17  
18  
19  
20  
21  
22  
23  
24  
25  
26  
27  
28  
29  
30  
31  
32  
33  
34  
35  
36  
37  
38  
39  
40  
41  
42  
43  
44  
45  
46  
47  
48  
49  
50  
51  
52  
53  
54  
55  
56  
57  
58  
59  
60

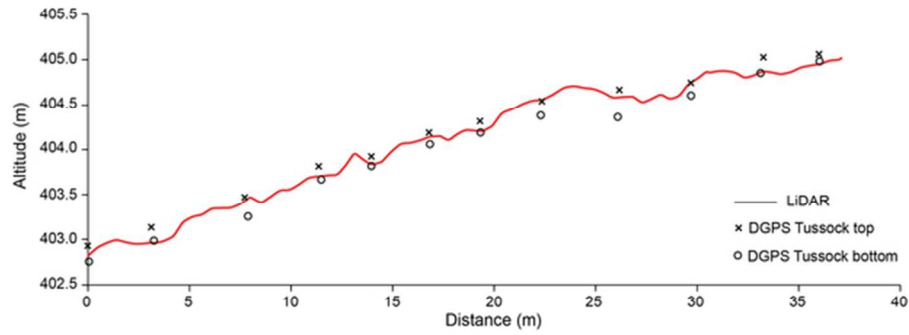


Figure 6: Alternate LiDAR topographic profile extracted from the wider TLS scan zone (figure 1) within Spooners catchment. DGPS Survey data describing the maximum and minimum vertical extent of dense vegetation components (tussocks) are included as paired measurements along the transect length.  
58x27mm (300 x 300 DPI)

1  
2  
3  
4  
5  
6  
7  
8  
9  
10  
11  
12  
13  
14  
15  
16  
17  
18  
19  
20  
21  
22  
23  
24  
25  
26  
27  
28  
29  
30  
31  
32  
33  
34  
35  
36  
37  
38  
39  
40  
41  
42  
43  
44  
45  
46  
47  
48  
49  
50  
51  
52  
53  
54  
55  
56  
57  
58  
59  
60

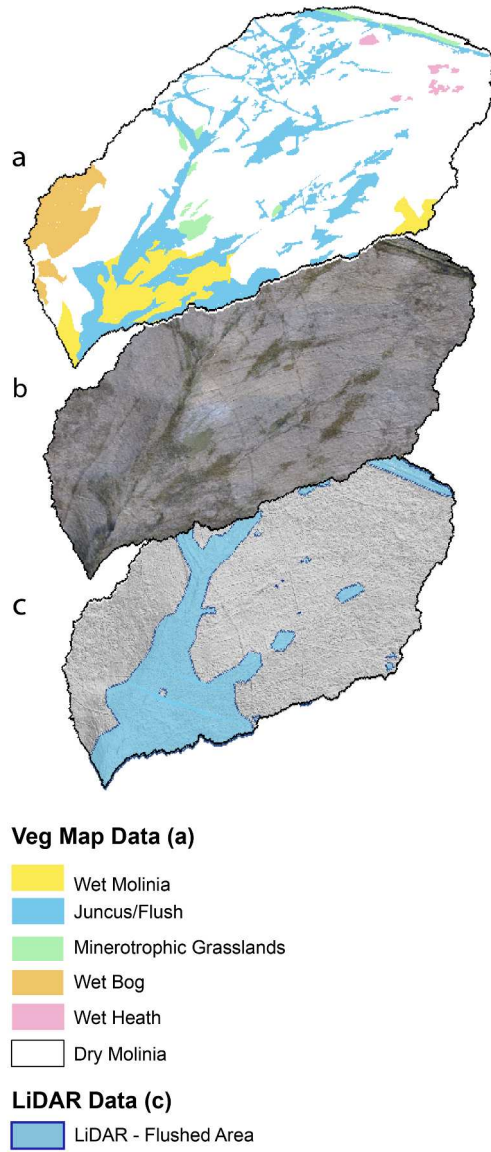


Figure 7: Habitat mapping of Aclands Catchment. (a) Vegetation communities digitised from aerial imagery. (b) High resolution aerial photograph. (c) Flushed vegetation Area delineated from classified LiDAR data. 184x415mm (300 x 300 DPI)

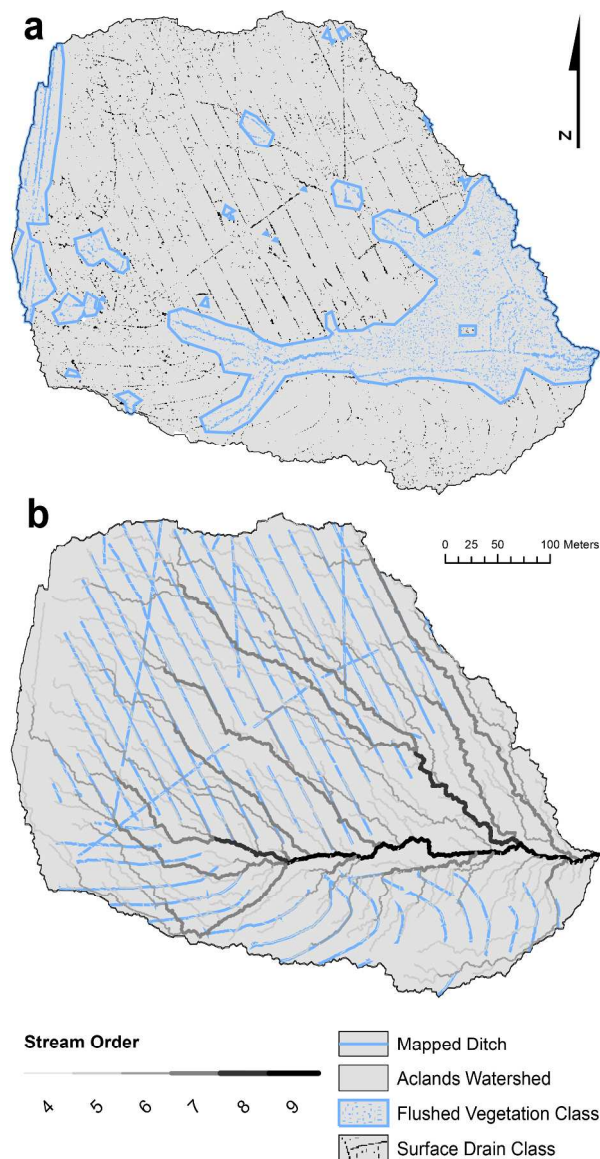


Figure 8: Mapping of surface drainage. (a) Data extracted from detrended LiDAR data (Aclands Catchment) and classified into surface drainage networks, whether natural or artificial (Black pixels) and rush dominated "flushed" zones (blue pixels). Pixels were classified using a threshold of pixel density. (b) A simple overland flow accumulation model with streams ordered using the Strahler classification (Strahler 1957) whereby stream size is classified according to a hierarchy of tributaries. A stream with no tributaries is 1st order; when two 1st order streams meet they subsequently form a 2nd order stream and so on. Only 4th to 9th order streams are displayed. 146x279mm (600 x 600 DPI)